Letter

Fine structure splitting cancellation in highly asymmetric InAs/InP droplet epitaxy quantum dots

N. R. S. van Venrooij , ^{1,2} A. R. da Cruz , ^{1,2} R. S. R. Gajjela , ² P. M. Koenraad , ² Craig E. Pryor, and Michael E. Flatté, 12,*

¹Department of Physics and Astronomy, University of Iowa, Iowa City, Iowa 52242, USA ²Department of Applied Physics, Eindhoven University of Technology, Eindhoven 5612 AZ, The Netherlands



(Received 27 September 2023; revised 7 February 2024; accepted 8 February 2024; published 15 May 2024)

We find the fine structure splitting (FSS) of a single exciton, which splits its degenerate ground-state manifold into singlets, nearly vanishes in highly asymmetric quantum dots (QDs) due to the cancellation of splitting effects with markedly different origin. The dots simulated are those that emerge on top of etch pits through the droplet epitaxy growth process; these etch pit dots break square (C_{4v}) spatial symmetry, which has been previously associated with small FSS. Configuration interaction calculations predict a vanishing FSS at a specific finite etch pit displacement from the center of the dot, for a structure far from square symmetry. We thus predict that highly asymmetric QDs may still display negligible FSS, providing avenues for high-fidelity generation of indistinguishable, polarization entangled photon pairs on demand.

DOI: 10.1103/PhysRevB.109.L201405

Optically active quantum dots (QDs) embedded in a solidstate matrix, which enables gate control (e.g., via strain tuning), can provide on-demand emission of indistinguishable, entangled polarization photon pairs as well as other elements of quantum technologies [1-3]. Given the right circumstances, the formation of a biexciton comprising two optically active (bright) excitons can lead to a recombination sequence in which two polarization-entangled photons are emitted. The mechanism behind this entanglement scheme is called the biexciton cascade [1,4,5]. The fidelity of entangled polarization photon pairs emitted from the dot, however, depends on the energetic splitting [so-called fine structure splitting (FSS)] between two bright exciton states [1,5,6], which are further split from two dark excitons by dark-bright splitting (DBS). In an optimal scenario, a QD lacking FSS would not provide any which-path information. This implies that it would be impossible to conclusively link an emitted photon to either of the two bright excitons, resulting in the entanglement of photons emitted afterward. Lowering the dot symmetry through growth kinetics from square (C_{4v}) to asymmetric (C_{2v}) , combined with the electron-hole exchange interaction [7,8], commonly provides the main source of this splitting [4,7]. Stranski-Krastanov (SK) growth [9] relies on surface strain to form QDs, therefore producing dots with highly elongated bases and large FSS [10]. Some growth techniques, such as droplet epitaxy (DE) [11], regularly produce embedded QDs with near C_{4v} symmetry [10,12,13]; many such dots are more symmetric and have smaller FSS than

Published by the American Physical Society under the terms of the Creative Commons Attribution 4.0 International license. Further distribution of this work must maintain attribution to the author(s) and the published article's title, journal citation, and DOI.

their SK counterparts [10,12]. However, DE growth suffers from the formation of etch pits: secondary structures at the base of the dot [12,14,15] which can break the structural symmetry of the dot and potentially increase the FSS. The complex interaction of the QD structure, exchange integrals, and the electron and hole wave functions forming the exciton produce several competing effects that have precise names within the literature [16,17], including long-range (LR) exchange, short-range (SR) exchange, and band mixing terms; few calculations have attempted to include all relevant terms in the FSS calculation or discuss their interplay.

Here, we identify an unexpected cancellation between FSS terms, denoted in the literature as (i) bulk band mixing, (ii) electric dipole, and (iii) SR exchange, that emerge from the Hartree-Fock Hamiltonian evaluated to second order in the electron-hole spatial separation. As a consequence, certain highly asymmetric dots exhibit negligible FSS. Our theoretical model utilizes an eight-band $\mathbf{k} \cdot \mathbf{p}$ envelope function theory to calculate the bound electron and hole wave functions for realistic QD geometries [18]. A configuration interaction (CI) calculation built from these states generates the single exciton energies and wave functions [19]. We find that simple etch pit structures break the exciton wave function symmetry and usually increase the FSS; however, certain highly asymmetric etch pit positions may be beneficial and reduce the FSS to near

A schematic of the simulated QD and etch pit is in Fig. 1; the dot has a base length of 24 nm, a height of 7 nm, facets on the (101), ($\overline{1}01$), (011), and (0 $\overline{1}1$) planes, and a diagonal baselength parallel to the (001) plane, coinciding with inferences from scanning tunneling microscopy (STM) measurements [15]. Because, in this letter, we are primarily focused on the effects of etch pits on the excitonic fine structure, we consider truncated square base QDs and neglect piezoelectric effects. For such dots, all the C_{4v} -symmetry-breaking effects are directly related to the positioning of the etch pit. The etch

^{*}michaelflatte@quantumsci.net

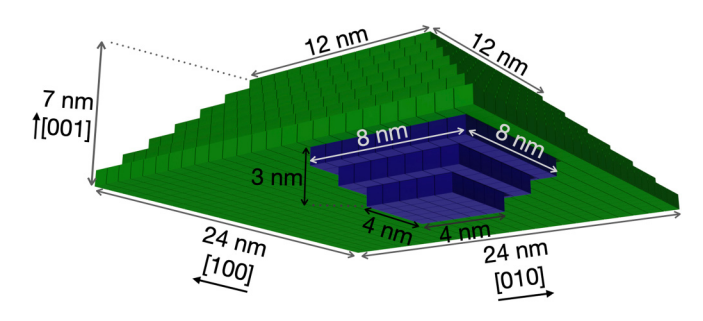


FIG. 1. Schematic diagram of the quantum dot (green) and etch pit (blue). Both structures are discretized on a grid with grid spacings of $1 \times 1 \times 1$ nm³.

pit shape was a truncated pyramid [20] with a base length of 8 nm and a height of 3 nm. The truncation of the pyramid was introduced due to insufficiently definitive data on the etch pit shape because the shape of a truncated pyramid is easier to parametrize and as it roughly approaches the etch pit shape measured experimentally using cross-sectional STM [15]. The QD and etch pit geometries are projected on a cubic grid with a grid size of 1 nm^3 . To study the effect that the etch pit position has on the QD fine structure, the etch pit was shifted along the diagonal to the corner of the QD base in increments of $\sqrt{2}$ nm.

The lowest-energy single-particle excited states of the dot correspond to adding an electron to the conduction states (electron) or removing an electron from the valence states (hole). The zone-center Bloch functions of the host material are a complete set of states; hence, any conduction or valence band states at finite crystal momentum can be expressed as linear combinations of them. The single particle states of the dot are calculated using an eight-band $\mathbf{k} \cdot \mathbf{p}$ envelope model described in Ref. [18]. Discrete states in the QD are expressed in terms of spatially varying coefficients (envelope functions) of the Bloch functions associated with the bulk conduction and valence zone-center Bloch functions (below referred to as conduction or valence contributions). Each of those electron and hole states has two spin orientations, and these four states form the smallest basis for a lowest-energy exciton manifold. In the absence of spin-dependent effects, the electron and hole spin degeneracy would produce four degenerate excitons at zero magnetic field. However, these four states are split through electronic interactions, which are dominated by the exchange interaction. We will thus focus on the four nondegenerate lowest-energy states of a single exciton, including the two spin states of the electron and hole constituents but excluding the biexciton and charged exciton states [1,19].

We orient our discussion of symmetry-breaking terms relative to the highest-symmetry case: spherical QDs. These have spin-degenerate lowest-energy electron ($S=\frac{1}{2}$) and fourfold degenerate lowest-energy hole states described by total angular momentum (spin and orbit) $J=\frac{3}{2}$ [21,22]. Without spin-dependent effects, this electron and hole degeneracy produces eight exciton states, corresponding to J=2 and 1. The symmetry of DE QDs is much lower; ideal DE QDs are truncated pyramids with a perfectly square base, described by C_{4v} symmetry, which breaks the fourfold degeneracy of the

lowest-energy hole. Depending on the QD dimensions, either the heavy hole (HH) or the light hole (LH) has lower energy. It is reported that short and wide QDs have the HH close to the band gap, whereas tall and narrow dots have the LH close to the band gap [23]. In this letter, we will solely focus on the former, which are more commonly grown.

These ideal DE QDs, in the presence of electron-electron interaction, exhibit four nondegenerate exciton eigenstates composed of combinations of the conduction band electrons and HH-band dominant holes. Among these excitons, there is a (near) degenerate high-energy pair with total angular momentum corresponding to $J \approx 1$ and a (near) degenerate low-energy pair with total angular momentum corresponding to $J \approx 2$. The order occurs because of the exchange interaction, which lowers the energy of parallel electron spins. A hole of a given spin (up/down) corresponds to a missing valence electron of opposite spin (down/up) and a remaining valence electron (up/down). The exchange energy of a conduction electron with the remaining valence electron will thus be lower if their spins are aligned, making the energy of the $J \approx 2$ exciton lower than that of $J \approx 1$. These total angular momentum values imply that all excitons have allowed optical transitions; however, the oscillator strengths of the high-energy $(J \approx 1)$ excitons greatly exceed those of the low-energy excitons, and thus, the high pair is often denoted as the bright pair, whereas the low-energy pair is referred to as the dim pair. Thus, the splitting between the bright pair and the dark pair is referred to as the dark-bright splitting (DBS). Selfassembled QDs will always have some effective elongation in one of the base diagonals due to strain-induced effects like piezoelectric fields [7]. This lowering of the symmetry further breaks the degeneracy of both pairs of excitons and introduces a FSS.

The electron and hole wave functions in this letter are computed using strain-dependent eight-band envelope function theory on a real-space grid. The QD electron and hole states can be written as a product between Bloch waves $\{u(\mathbf{r})\}$ and spatially varying envelope functions $\{F(\mathbf{r}), G(\mathbf{r})\}$. The envelopes themselves are approximately constant within one unit cell of the grid and depend on the discrete grid coordinate \mathbf{R} . The Bloch functions vary over a unit cell and are periodic, so they depend solely on the continuous coordinate $\tilde{\mathbf{r}}$ within a unit cell. The position vector may then be written as $\mathbf{r} = \mathbf{R} + \tilde{\mathbf{r}}$. We then compute the confined electron and hole states, which depend on the composition of the QD and its geometry. The electron and hole wave functions are

$$\psi_{e}(\mathbf{R}, \tilde{\mathbf{r}}) = \sum_{i=1}^{8} F_{i}(\mathbf{R}) u_{i}(\tilde{\mathbf{r}}),$$

$$\psi_{h}(\mathbf{R}, \tilde{\mathbf{r}}) = \sum_{j=1}^{8} G_{j}(\mathbf{R}) u_{j}(\tilde{\mathbf{r}}),$$
(1)

with ψ_e and ψ_h the electron and hole wave functions, respectively, F_i the electron envelope functions, G_j the hole envelope functions, and u_i the Bloch functions corresponding to each band (using the basis of Ref. [24], see Supplemental Material [25]) [26–29]. To calculate the eigenenergy of an exciton and to account for the antisymmetrization requirement of a

two-body fermionic wave function, the wave functions in Eq. (1) are the two-particle Slater determinants [19,30]:

$$\Psi_{eh}(\mathbf{R}_{1}, \tilde{\mathbf{r}}_{1}, \mathbf{R}_{2}, \tilde{\mathbf{r}}_{2})$$

$$= \frac{1}{\sqrt{2}} [\psi_{e}(\mathbf{R}_{1}, \tilde{\mathbf{r}}_{1})\psi_{h}(\mathbf{R}_{2}, \tilde{\mathbf{r}}_{2}) - \psi_{e}(\mathbf{R}_{2}, \tilde{\mathbf{r}}_{2})\psi_{h}(\mathbf{R}_{1}, \tilde{\mathbf{r}}_{1})]$$

$$= \frac{1}{\sqrt{2}} \sum_{i,j=1}^{8} [F_{i}(\mathbf{R}_{1})u_{i}(\tilde{\mathbf{r}}_{1})G_{j}(\mathbf{R}_{2})u_{j}(\tilde{\mathbf{r}}_{2})$$

$$- F_{i}(\mathbf{R}_{2})u_{i}(\tilde{\mathbf{r}}_{2})G_{i}(\mathbf{R}_{1})u_{i}(\tilde{\mathbf{r}}_{1})]. \tag{2}$$

An upper bound on the eigenenergy of the exciton is obtained from the expectation value of the Hartree-Fock Hamiltonian:

$$\hat{\mathcal{H}}_{HF} = E_e + E_h + \frac{e^2}{4\pi\epsilon_0 \varepsilon_\infty} \frac{1}{||\Delta \mathbf{R} + \Delta \tilde{\mathbf{r}}||}, \quad (3)$$

with E_e and E_h the eigenenergies of the electron and hole, e the elementary charge, ϵ_0 the vacuum permittivity, ϵ_∞ the high frequency (greater than phonon excitation energies) dielectric constant, $\Delta \mathbf{R} = \mathbf{R}_1 - \mathbf{R}_2$, and $\Delta \tilde{\mathbf{r}} = \tilde{\mathbf{r}}_1 - \tilde{\mathbf{r}}_2$. For a two-particle fermionic wave function, the Coulomb interaction can be split into the Hartree contribution J and the exchange contribution K.

For the four excitons constructed from two electron and two hole states, the specific states must be labeled; a specific one-particle (electron or hole) or two-particle (exciton) state will be labeled with the index ℓ to distinguish this label from the band indices i and j. The Hamiltonian in Eq. (3) will mix the four different exciton states so a matrix Schrödinger equation is constructed in the CI calculation. The excitonic eigenfunctions Φ are written as a linear combination of the Slater determinants in Eq. (2):

$$\Phi_{\ell}(\mathbf{R}_1, \tilde{\mathbf{r}}_1, \mathbf{R}_2, \tilde{\mathbf{r}}_2) = \sum_{\ell'=1}^{4} C_{\ell'} \Psi_{\ell'}(\mathbf{R}_1, \tilde{\mathbf{r}}_1, \mathbf{R}_2, \tilde{\mathbf{r}}_2).$$
 (4)

Off-diagonal matrix elements between different Slater determinants originate from exchange. The Hamiltonian matrix elements for the CI calculation are

$$\langle \Psi_{\ell} | \hat{\mathcal{H}}_{HF} | \Psi_{\ell'} \rangle = (E_e - E_h) \delta_{\ell,\ell'} - \mathcal{J}_{\ell,\ell'} + \mathcal{K}_{\ell,\ell'}, \quad (5)$$

where $\mathcal{J}_{\ell,\ell'}$ is the Hartree contribution and $\mathcal{K}_{\ell,\ell'}$ is the exchange contribution. Computing these matrix elements and diagonalizing this Hamiltonian results in an upper bound for the exciton eigenenergies.

Within the theoretical framework of an envelope function model, the electron-hole exchange interaction is conveniently divided into two main constituents denoted SR and LR [16,17], indicating whether the Coulomb interaction occurs between an electron and a hole within the same unit cell or in two different unit cells. The interaction within a unit cell ($\mathbf{R}_1 = \mathbf{R}_2 = \mathbf{R}$) corresponds to the analytic part of the exchange interaction or the SR exchange interaction [31–34]. The interaction across different unit cells ($\mathbf{R}_1 \neq \mathbf{R}_2$) is referred to as the nonanalytic part of the exchange interaction or the LR exchange interaction [32–34]. A more detailed description of the exchange interaction is given in the Supplemental Material [25].

Terms in the LR interaction can be further subdivided into the second-order dipolar interaction $[\mathcal{K}_{LR,DD}^{(2)}]$ and other, usually neglected, zeroth-, first-, and second-order band mixing interactions $[\mathcal{K}_{LR,BM}^{(0)},\mathcal{K}_{LR,BM}^{(1)},$ and $\mathcal{K}_{LR,BM}^{(2)}$, respectively]. This results in the following expression:

$$\mathcal{K}_{LR} = \mathcal{K}_{LR,BM}^{(0)}(||\Delta \mathbf{R}||^{-1}) + \mathcal{K}_{LR,BM}^{(1)}(||\Delta \mathbf{R}||^{-2})
+ \mathcal{K}_{LR,DD}^{(2)}(||\Delta \mathbf{R}||^{-3}) + \mathcal{K}_{LR,BM}^{(2)}(||\Delta \mathbf{R}||^{-3}),$$
(6)

where $\mathcal{K}_{LR,BM}^{(0)}$, $\mathcal{K}_{LR,BM}^{(1)}$, and $\mathcal{K}_{LR,BM}^{(2)}$ are, respectively, the zeroth-, first-, and second-order band mixing interactions. These interactions exclusively occur in models where the electron and hole wave functions have contributions from both conduction and valence bands. The term $\mathcal{K}_{LR,DD}^{(2)}$ is the more frequently used dipole interaction for multiband wave functions. Even though the zeroth- and first-order band mixing terms drop off more slowly than the dipole interaction, the contribution of the dipole interaction to the FSS is still larger. Nevertheless, the band mixing contributions to wave functions can be large, even in spherical dots, approaching $\sim 30\%$ [21,35]. Thus, the band mixing components cannot be ignored as will become evident below.

The FSS of QDs has been previously investigated using the SR exchange interaction [3,36], assuming the electron and hole wave functions are composed purely of conduction and valence band components, respectively. In this case, the exchange interaction takes the form [31]:

$$\mathcal{K}_{SR} = \Delta \mathbf{S}_{\Gamma_6} \cdot \mathbf{J}_{\Gamma_8}, \tag{7}$$

where \mathbf{S}_{Γ_6} is the spin operator for the bottom of the conduction band, \mathbf{J}_{Γ_8} is the spin- $\frac{3}{2}$ operator for the top of the valence band, and the magnitude Δ is fit to experiment. This form may be deduced from the fact that $\mathbf{S} \cdot \mathbf{J}$ is the only available rotationally invariant operator.

In an eight-band model, however, there are three rotationally invariant operators: $\mathbf{S}_{\Gamma_6} \cdot \mathbf{J}_{\Gamma_8}$, $\mathbf{S}_{\Gamma_6} \cdot \mathbf{S}_{\Gamma_7}$, and $\mathbf{S}_{\Gamma_7} \cdot \mathbf{J}_{\Gamma_8}$, where \mathbf{S}_{Γ_7} is the spin operator for the spin-orbit band. Each of these three interactions has its own coefficient determined by the integral in Eq. (9) of the Supplemental Material [25], which would be fit to experiment. Lacking sufficient data to do such a fit forces us to only consider the interaction $\mathbf{S}_{\Gamma_6} \cdot \mathbf{J}_{\Gamma_8}$. This is a reasonable assumption considering that the contribution of the Γ_7 bands to each of the wave functions is typically <1%.

The effect of the etch pit position on the fine structure of the bright excitons can be seen in Fig. 2, which presents the main results of this letter. The figure shows the calculated FSS between the bright exciton states for three different situations: the total exchange interaction, only band mixing interactions, and only dipole interactions. As the etch pit is shifted further along the diagonal, the FSS gradually increases until it reaches a maximum, then decreases, passes through zero, and turns negative.

The origin for this behavior may be explained by comparing the band mixing contributions to the FSS with the dipole contributions. The cancelation of FSS occurs because of the opposite sign of the $\mathcal{K}_{LR,DD}^{(2)}$ term (lower right panel Fig. 3) to the other terms; this originates from the second term in Eq. (6) of the Supplemental Material, and requires a substantial extent of the dot in two directions, but not

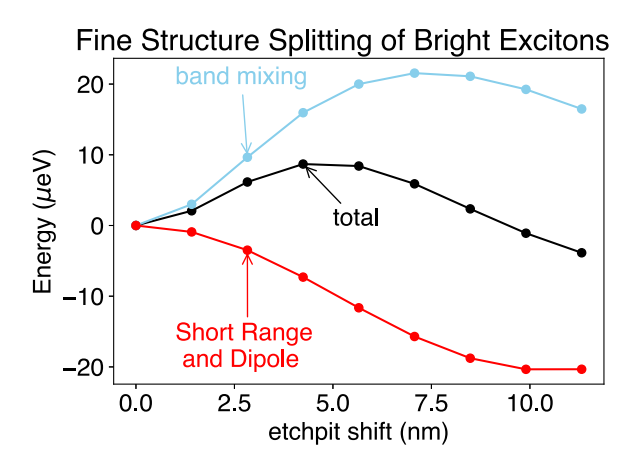


FIG. 2. The fine structure splitting (FSS) between the bright excitons for a droplet epitaxy quantum dot. The FSS is defined as $\text{FSS}_{\text{bright}} = E_{\text{brights}} - E_{\text{bright}}$. The black line indicates the calculated FSS for the total exchange interaction. The blue line indicates the calculated FSS when solely including the band mixing terms of the exchange interaction; these are $\mathcal{K}_{\text{LR,BM}}^{(0)}$, $\mathcal{K}_{\text{LR,BM}}^{(1)}$, and $\mathcal{K}_{\text{LR,BM}}^{(2)}$. The red line indicates the calculated FSS when solely including the short-range (\mathcal{K}_{SR}) and dipole ($\mathcal{K}_{\text{LR,DD}}^{(2)}$) interactions.

a third. Thus this cancelation emerges in the flat dots that we consider here. A more detailed description on how each contribution to the exchange interaction acts separately on the FSS can be seen in Fig. 3; however, a full discussion of all the nuances is beyond the scope of this letter. Figure 3 identifies the dipole interaction as the largest contributor to the bright exciton FSS. The magnitude of the zeroth-order band mixing interaction is approximately the same as that of the SR exchange interaction, and both are smaller than the magnitude of the first-order band mixing interaction. Thus, ignoring the band mixing contributions leads to significantly incorrect exciton FSS values. Figure 3 shows that the dark exciton FSS (FSS $_{\text{dark}} = E_{\text{dim}} - E_{\text{dark}}$) is not affected nearly as much by the presence of an etch pit as the bright excition FSS.

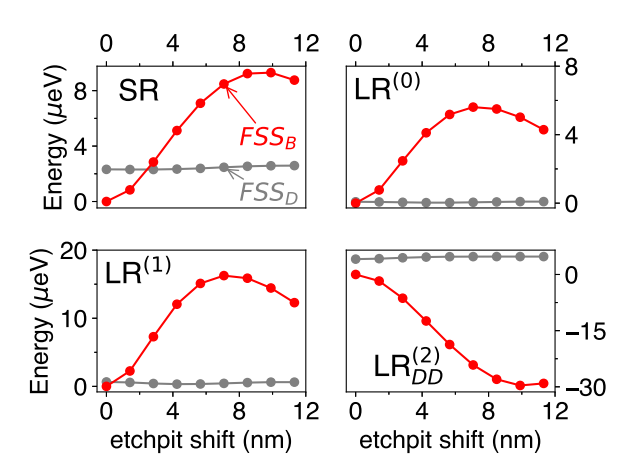


FIG. 3. The contributions of each part of the exchange interaction to the fine structure splitting of both the bright (red) and the dark (gray) excitons. It is evident from all plots that the bright states are predominantly affected by the exchange interaction, whereas the dark states are not.

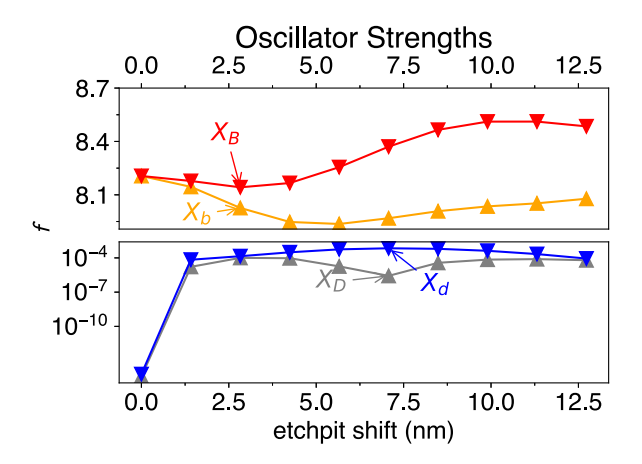


FIG. 4. Oscillator strengths for the bright (red) and dark (gray) excitons as a function of the etch pit position. With a centered etch pit, the bright excitons have equal oscillator strengths, but as the pit shifts, one (X_B) becomes slightly brighter than the other (X_b) . For zero etch pit shift, the dark excitons have zero oscillator strength to within the numerical accuracy of the calculations. As the pit shifts, the dark excitons become merely dim (X_D) and (X_D) .

The bright vs dark excitons are identified from the oscillator strengths of each exciton, calculated for each etch pit position and shown in Fig. 4. Each exciton is labeled according to its oscillator strength. For the bright excitons, the exciton with the largest oscillator strength is labeled X_B , whereas the exciton with the second-largest oscillator strength is labeled X_b . The exciton with the second-lowest oscillator strength is referred to as the dim exciton and is labeled X_d , whereas the dark has the lowest oscillator strength and is labeled X_D . The effect of shifting the etch pit on the exciton oscillator strengths is dramatic, especially for the dark and

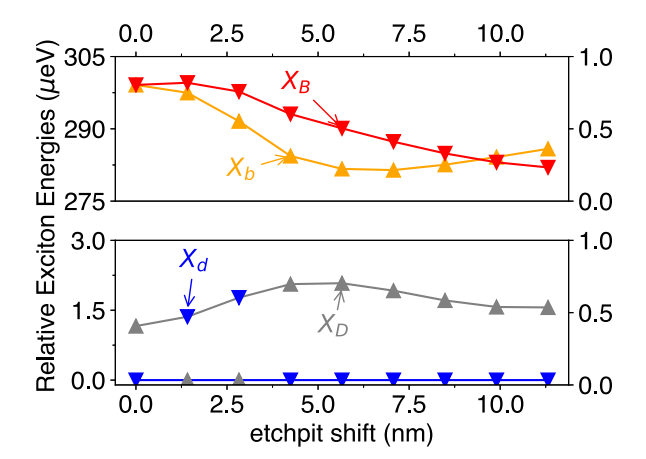


FIG. 5. Energies of an exciton in a quantum dot which has a varying etch pit position, relative to the ground-state exciton. The top figure shows the two bright excitons (X_b, X_B) , which are always higher in energy. The lowest-energy exciton can be either the dark exciton (X_D) or the dim exciton (X_d) . The bottom figure shows the splitting between these two and indicates which is the ground-state exciton.

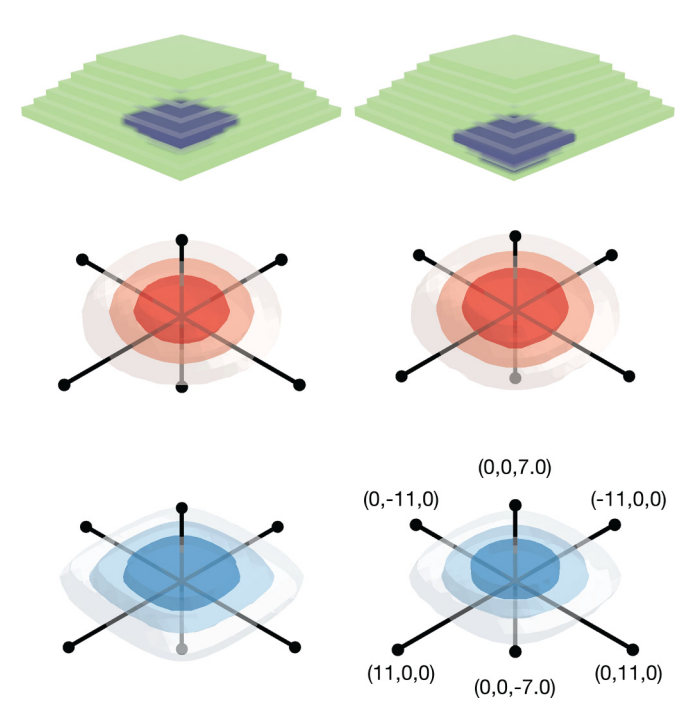


FIG. 6. Single-particle electron (red) and hole (blue) states for two different etch pit positions. Above the states, the quantum dot (QD) and etch pit geometries are depicted schematically (not to scale of the states). The states on the left correspond to a QD with a centered etch pit, while the states on the right correspond to a QD with its etch pit shifted along the diagonal by 8.49 nm, whose FSS is 2.35 μ eV. The innermost isosurfaces are set at 30% of the maximum probability density, with each subsequent isosurface at 30% probability density of the previous isosurface. Lines along symmetry axes intersect at the dot center; fixed positions are labeled with black points and their positions relative to the center in units of nm.

dim states. For a centered etch pit, both dark states have a negligible oscillator strength; thus, it is not possible to label the states dark and dim. As the etch pit is shifted further away from the center, the oscillator strengths increase approximately five orders of magnitude, however, remain far smaller than those of the bright states. Therefore, the dark and bright states do not switch their identification for these dots. By comparing the results of Figs. 4 and 3, we see the presence of an etch pit significantly increases the oscillator strengths of the dark exciton without affecting the dark exciton FSS. Thus, such etch pits may improve dark exciton qubit performance [37,38].

Figure 5 shows the exciton energies with the lowest-energy exciton subtracted from the other exciton energies. The bright excitons are higher in energy than the dark excitons since the electron-hole exchange interaction acts repulsively on antiparallel spin configurations. Figure 6 shows maps of the single-particle states of a QD with an etch pit at two different locations. When the etch pit is shifted off-center such that C_{4v} symmetry is broken, this causes the electron and hole states to respond to this shift by either moving toward the etch pit region (electrons) or away from it (holes).

The degeneracy of the bright excitons is a necessary condition for high fidelity between emitted photons; however, the fidelity can be degraded by other effects such as those originating from charge and spin noise. As these band mixing terms have led to FSS cancellation in asymmetric structures, we suggest other dot geometries may also produce unexpected features in the exciton fine structure.

N.R.S.v.V. and M.E.F. acknowledge useful discussions with M. Atatüre and P. Klenovský and the support of National Science Foundation Grant No. DMR-1921877.

- [1] R. M. Stevenson, R. J. Young, P. Atkinson, K. Cooper, D. A. Ritchie, and A. J. Shields, A semiconductor source of triggered entangled photon pairs, Nature (London) 439, 179 (2006).
- [2] D. J. Norris, A. L. Efros, M. Rosen, and M. G. Bawendi, Size dependence of exciton fine structure in CdSe quantum dots, Phys. Rev. B 53, 16347 (1996).
- [3] L. Landin, M. E. Pistol, C. Pryor, M. Persson, L. Samuelson, and M. Miller, Optical investigations of individual InAs quantum dots: Level splittings of exciton complexes, Phys. Rev. B 60, 16640 (1999).
- [4] R. Singh and G. Bester, Lower bound for the excitonic fine structure splitting in self-assembled quantum dots, Phys. Rev. Lett. 104, 196803 (2010).
- [5] N. Akopian, N. H. Lindner, E. Poem, Y. Berlatzky, J. Avron, D. Gershoni, B. D. Gerardot, and P. M. Petroff, Entangled photon pairs from semiconductor quantum dots, Phys. Rev. Lett. 96, 130501 (2006).
- [6] D. Huber, M. Reindl, J. Aberl, A. Rastelli, and R. Trotta, Semiconductor quantum dots as an ideal source of polarizationentangled photon pairs on-demand: A review, J. Opt. 20, 073002 (2018).
- [7] R. Seguin, A. Schliwa, S. Rodt, K. Pötschke, U. W. Pohl, and D. Bimberg, Size-dependent fine-structure splitting in

- self-organized InAs/GaAs quantum dots, Phys. Rev. Lett. 95, 257402 (2005).
- [8] M. Bayer, G. Ortner, O. Stern, A. Kuther, A. A. Gorbunov, A. Forchel, P. Hawrylak, S. Fafard, K. Hinzer, T. L. Reinecke *et al.*, Fine structure of neutral and charged excitons in self-assembled In(Ga)As/(Al)GaAs quantum dots, Phys. Rev. B 65, 195315 (2002)
- [9] C. Schneider, S. Höfling, and A. Forchel, Growth of III-V semiconductor quantum dots, in *Quantum Dots: Optics, Electron Transport and Future Applications*, edited by A. Tartakovskii (Cambridge University Press, Cambridge, 2012), p. 3–20.
- [10] J. Skiba-Szymanska, R. M. Stevenson, C. Varnava, M. Felle, J. Huwer, T. Müller, A. J. Bennett, J. P. Lee, I. Farrer, A. B. Krysa *et al.*, Universal growth scheme for quantum dots with low fine-structure splitting at various emission wavelengths, Phys. Rev. Appl. 8, 014013 (2017).
- [11] M. Gurioli, Z. Wang, A. Rastelli, T. Kuroda, and S. Sanguinetti, Droplet epitaxy of semiconductor nanostructures for quantum photonic devices, Nat. Mater. 18, 799 (2019).
- [12] R. S. R. Gajjela and P. M. Koenraad, Atomic-scale characterization of droplet epitaxy quantum dots, Nanomaterials 11, 85 (2021).
- [13] R. S. R. Gajjela, E. M. Sala, J. Heffernan, and P. M. Koenraad, Control of morphology and substrate etching in

- InAs/InP droplet epitaxy quantum dots for single and entangled photon emitters, ACS Appl. Nano Mater. **5**, 8070 (2022).
- [14] J. Keizer, J. Bocquel, P. Koenraad, T. Mano, T. Noda, and K. Sakoda, Atomic scale analysis of self assembled GaAs/AlGaAs quantum dots grown by droplet epitaxy, Appl. Phys. Lett. 96, 062101 (2010).
- [15] R. S. R. Gajjela, N. R. S. van Venrooij, A. R. da Cruz, J. Skiba-Szymanska, R. M. Stevenson, A. J. Shields, C. E. Pryor, and P. M. Koenraad, Study of size, shape, and etch pit formation in InAs/InP droplet epitaxy quantum dots, Nanotechnology 33, 305705 (2022).
- [16] V. Křápek, P. Klenovský, and T. Šikola, Excitonic fine structure splitting in type-II quantum dots, Phys. Rev. B 92, 195430 (2015).
- [17] T. Takagahara, Theory of exciton doublet structures and polarization relaxation in single quantum dots, Phys. Rev. B 62, 16840 (2000).
- [18] C. Pryor, Eight-band calculations of strained InAs/GaAs quantum dots compared with one-, four-, and six-band approximations, Phys. Rev. B 57, 7190 (1998).
- [19] A. Franceschetti, H. Fu, L. W. Wang, and A. Zunger, Manybody pseudopotential theory of excitons in InP and CdSe quantum dots, Phys. Rev. B **60**, 1819 (1999).
- [20] M. Zocher, C. Heyn, and W. Hansen, Droplet etching with indium—Intermixing and lattice mismatch, J. Cryst. Growth **512**, 219 (2019).
- [21] P. C. Sercel and K. J. Vahala, Analytical formalism for determining quantum-wire and quantum-dot band structure in the multiband envelope-function approximation, Phys. Rev. B 42, 3690 (1990).
- [22] A. L. Vartanian, A. L. Asatryan, and A. A. Kirakosyan, The polaronic shift of exciton binding energy in quantum dots with a degenerate valence band, J. Phys.: Condens. Matter 14, 13357 (2002).
- [23] M. Jeannin, A. Artioli, P. Rueda-Fonseca, E. Bellet-Amalric, K. Kheng, R. André, S. Tatarenko, J. Cibert, D. Ferrand, and G. Nogues, Light-hole exciton in a nanowire quantum dot, Phys. Rev. B 95, 035305 (2017).
- [24] T. B. Bahder, Eight-band k·p model of strained zinc-blende crystals, Phys. Rev. B 41, 11992 (1990).
- [25] See Supplemental Material at https://link.aps.org/supplemental/ 10.1103/PhysRevB.109.L201405 for additional detail on the exchange interaction expressions and includes Refs. [26–29].

- [26] J. J. Sakurai and R. L. Liboff, Modern quantum mechanics, Am. J. Phys. 54, 668 (1986).
- [27] I. Vurgaftman, J. R. Meyer, and L. R. Ram-Mohan, Band parameters for III-V compound semiconductors and their alloys, J. Appl. Phys. 89, 5815 (2001).
- [28] U. Banin, J. Lee, A. Guzelian, A. Kadavanich, and A. Alivisatos, Exchange interaction in InAs nanocrystal quantum dots, Superlattices Microstruct. 22, 559 (1997).
- [29] O. Madelung, U. Rössler, and M. Schulz, Indium arsenide (InAs), band structure, energies of symmetry points, *Landolt-Börnstein—Group III Condensed Matter* 41A1β (Springer-Verlag, Berlin, 2002).
- [30] J.-W. Luo, G. Bester, and A. Zunger, Long- and short-range electron-hole exchange interaction in different types of quantum dots, New J. Phys. 11, 123024 (2009).
- [31] G. Bir and G. Pikus, Symmetry and Strain-Induced Effects in Semiconductors (John Wiley & Sons, Hoboken, 1974), p. 484.
- [32] A. Franceschetti, L. W. Wang, H. Fu, and A. Zunger, Short-range versus long-range electron-hole exchange interactions in semiconductor quantum dots, Phys. Rev. B 58, R13367(R) (1998).
- [33] J. W. Luo, A. Franceschetti, and A. Zunger, Direct-bandgap InAs quantum-dots have long-range electron-hole exchange whereas indirect gap Si dots have short-range exchange, Nano Lett. 9, 2648 (2009).
- [34] S. V. Goupalov and E. L. Ivchenko, Electron-hole long-range exchange interaction in semiconductor quantum dots, J. Cryst. Growth **184–185**, 393 (1998).
- [35] J. van Bree, A. Y. Silov, P. M. Koenraad, and M. E. Flatté, Spin-orbit-induced circulating currents in a semi-conductor nanostructure, Phys. Rev. Lett. 112, 187201 (2014).
- [36] A. L. Efros, M. Rosen, M. Kuno, M. Nirmal, D. J. Norris, and M. Bawendi, Band-edge exciton in quantum dots of semiconductors with a degenerate valence band: Dark and bright exciton states, Phys. Rev. B 54, 4843 (1996).
- [37] M. Holtkemper, G. F. Quinteiro, D. E. Reiter, and T. Kuhn, Dark exciton preparation in a quantum dot by a longitudinal light field tuned to higher exciton states, Phys. Rev. Res. 3, 013024 (2021).
- [38] M. Zieliński, Y. Don, and D. Gershoni, Atomistic theory of dark excitons in self-assembled quantum dots of reduced symmetry, Phys. Rev. B 91, 085403 (2015).